Journal of Hydrology 574 (2019) 467–475

Contents lists available at ScienceDirect

Journal of Hydrology

journal homepage: www.elsevier.com/locate/jhydrol

Research papers

# Early twenty-first century glacier mass losses in the Indus Basin constrained by density assumptions

Sher Muhammad[a,b,*], Lide Tian[a,c,d,e,*], Asif Khan[f,g,h]

[a] Institute of International Rivers and Eco-security, Yunnan University, Kunming 650500, China
[b] International Centre for Integrated Mountain Development (ICIMOD), GPO Box 3226, Kathmandu, Nepal
[c] Key Laboratory of Tibetan Environmental Change and Land Surface Processes, Chinese Academy of Sciences, Beijing 100101, China
[d] Yunnan Key Laboratory of International Rivers and Transboundary Eco-security, Yunnan University, Kunming 650500, China
[e] College of Resource and Environment, University of Chinese Academy of Sciences, Beijing 100190, China
[f] Department of Engineering, University of Cambridge, Trumpington Street, CB3 1PZ, UK
[g] Department of Civil Engineering, University of Engineering and Technology, Peshawar, Jalozai Campus, Pakistan
[h] Water Informatics Centre, LUMS, Lahore, Pakistan

ARTICLE INFO

This manuscript was handled by Marco Borga, Editor-in-Chief, with the assistance of Massimiliano Zappa, Associate Editor

*Keywords:*
Remote sensing
Mass balance
Density assumptions
Indus Basin
Karakoram

ABSTRACT

Glaciers in the upper Indus supply more than half of the river water, are experiencing significant melting with a debated fate. The recent melting rate is still contained by considerable uncertainties, hindering to estimate precise glacier mass change. Here we present geodetic mass balance results for the whole Indus Basin using SRTM and ALOS 30 m elevation data, improved glacier inventory, optimized glacier surface density, and validation through in-situ differential GPS and ICESat data. Our glacier inventory and derived by improving RGI6.0 boundaries and separated into debris cover and debris free parts. The derived surface elevation changes were converted into annual mass balances using separated density assumptions (four criteria) for debris-covered ice ($900 \pm 60\,kg\,m^{-3}$), debris-free ice (below 20° and 25° slopes ($850 \pm 60\,kg\,m^{-3}$) and above 20° and 25° slopes ($600 \pm 60\,kg\,m^{-3}$)), respectively. The resulting mass balance biased between $-0.20$ and $0.09\,m$ water equivalent (w.e.) $a^{-1}$ using an average ($850 \pm 60\,kg\,m^{-3}$) density assumption throughout the Indus Basin. In the western Himalaya and Hindu Kush, the glacier mass losses are less affected by the average density assumption compared to the Karakoram. The western (Hunza) and central (Shigar) Karakoram glaciers show negligible mass losses of $-0.02 \pm 0.12$ and $-0.01 \pm 0.13\,m\,w.e.\,a^{-1}$ in contrast to the relatively more negative mass balance ($-0.26 \pm 0.21\,m\,w.e.\,a^{-1}$) in the eastern (Shyok) Karakoram. All the sub-basins exhibit negative mass balances, with the most negative values ranging from $-0.34 \pm 0.31$ to $0.44 \pm 0.27\,m\,w.e.\,a^{-1}$ in the Ravi, Chenab and Jhelum sub-basins of the Himalaya. The whole Indus Basin contributes approximately $+0.014 \pm 0.016\,mm\,a^{-1}$ to the global mean sea-level equivalent.

## 1. Introduction

The total water supply contributed approximately 50% by snow and glaciers (Winiger et al., 2005). Per capita water availability in Pakistan has decreased from 5260 cubic meters in 1951 to below 1000 cubic meters in 2016 (National Water Policy, 2018) mainly due to demographic growth and mismanagement. Glaciers will continue to experience substantial ice loss, with the major losses in the Indus Basin (Shrestha et al., 2015). The increased melting has a high probability of hazards/disasters (Tian et al., 2017), downstream flooding (Lutz et al., 2016; Milner et al., 2017), which may cause economic losses and casualties (Haq et al., 2012; Memon et al., 2015), and therefore requires careful monitoring.

Glaciers are mostly observed using remote sensing instruments, but most of the studies do not provide full spatial coverage (e.g., Gardelle et al., 2013; Kääb et al., 2015, 2012). Most importantly, the majority of previous studies used constant densities for volume to mass change estimations (Bolch et al., 2017; Gardelle et al., 2013, 2012a; Kääb et al., 2015; Zhou et al., 2017). Although, a recent study extended the spatial and temporal coverage of glacier observations in the High Mountain Asia (HMA) (Brun et al., 2017), the study used constant ice densities and existing inventories that may contain significant uncertainties in regions where glaciers are mostly accumulating in steep terrain and the density is significantly lower (Hewitt, 2011, 1998). In addition, the

* Corresponding authors at: Institute of International Rivers and Eco-security, Yunnan University, Kunming 650500, China.
*E-mail addresses:* msher@ynu.edu.cn (S. Muhammad), ldtian@ynu.edu.cn (L. Tian).

https://doi.org/10.1016/j.jhydrol.2019.04.057
Received 22 July 2018; Received in revised form 27 March 2019; Accepted 16 April 2019
Available online 23 April 2019

glacier-wide density is also expected to be smaller (Huss, 2013) than the widespread average density applied. The average density assumption for volume to mass conversion represents a potential source of error (Zemp et al., 2010). Huss (2013) shows that the constant density assumptions also have substantial variability in geodetic mass balance measurements constrained by short temporal coverage.

In this study, we emphasize the sensitivity of ice density assumptions for volume to mass change conversion, particularly in the upper part of the glaciers. The Shuttle Radar Topographic Mission (SRTM), Advanced Land Observing Satellite (ALOS) 30 m elevation data and the latest available glacier boundaries (RGI6.0) that were improved and separated into debris-covered and debris-free part (Kraaijenbrink et al., 2017) in this study, fulfilled our objective. ICESat and dGPS data helped to validate (Wesche et al., 2009) the glacier mass balance results. This study provides estimates of volume to mass change estimates on sub-basin scale using separated densities for the debris-covered and debris-free as well as area below and above 20° and 25° slope of glaciers and improved glacier boundaries. This allows us to estimate the contribution to discharge in the Indus river as well as sea-level rise.

## 2. Study area

The trunk of the Indus River originates in the western Tibetan Plateau, flows through Ladakh, and Zanskar river located in the Indian administered part of Kashmir before entering the mountain areas of Gilgit-Baltistan administered by Pakistan and enters the Arabian Sea. Its total catchment area is more than 1.1 million km$^2$, with the upper part comprising the Hindu Kush, Karakorum, and Himalayan ranges. The headwaters of the Indus River are in Shiquanhe on the western Tibetan Plateau, and the river then merges with the Satluj, Beas, Ravi, Chenab, Kharmong, Shyok, Shingo, Jhelum, Astore, Shigar, Hunza, Upper Indus, Gilgit, Swat, and Kabul rivers. Karakoram, Himalaya, and Hindukush cover approximately 58%, 30%, and 12% of the glaciers, respectively (RGI Consortium, 2017). The basin provides water for commercial and domestic consumption by the downstream population. Millions of people living downstream are directly or indirectly dependent on Indus River water. The climate of the upper Indus is characterized by sub-Mediterranean circulation from the west, summer monsoon and the anticyclone from Tibet (Hewitt, 2011, 1998; Lutz et al., 2016; Maussion et al., 2014). The upper portions of the Indus Basin can be classified into high-elevation (glaciers) areas, moderate-elevation (seasonally snow covered) areas and low-elevation (rain-fed) valley floors (Archer, 2003). Fig. 1 shows a map of the study area.

## 3. Methodology

The study uses SRTM, ALOS, ICESat, and dGPS data. The method to process these data comprises of four parts: i) glacier outline extraction, separation into debris-covered and debris-free, ii) geometric correction, iii) SRTM C-band penetration correction, iv) surface elevation change and mass balance and v) inter-comparison of ALOS, SRTM, ICESat and dGPS data and uncertainty estimation. The method for updating glacier inventory (separated into debris-covered and debris-free) is described in Supplementary material. The details of selected methodological steps are described in the following section.

### 3.1. Geometric correction

The geodetic method of digital elevation model (DEM) differencing was used to estimate mass balance from the SRTM-C and ALOS DEMs, which both have spatial resolutions of 30 m. Before differencing the DEMs, a co-registration was performed to overlay and compare each pixel of both data sets optimally. A systematic half-pixel planimetric bias existed in the ALOS DEM compared to the SRTM owing to the definition of the pixel location (corner vs. center). Therefore, a shift of 12.73 m and 15.40 m (approximately equivalent to half a pixel) was applied to the easting and northing directions, respectively, of the ALOS DEM using the shift tool in ArcGIS. After the shift, the DEM were differenced and compared on different aspects over non-glacier terrain (Gardelle et al., 2013). This process follows the methodology of Nuth and Kääb (2011) to correct geometric and elevation dependent biases for all the sub-basins. The altitude dependent biases were corrected for each sub-basin applying an average value for each 100 m elevation bin. The elevation difference over non-glacier areas was compared using the ALOS and SRTM data. The distribution of off-glacier height differences is within ± 20 m difference which is expected in a rugged topography (Berthier et al., 2006; Kääb, 2005) and cause negligible average surface elevation change after removing the outliers.

### 3.2. SRTM C-band penetration correction

One of the major problems associated with SRTM data to estimate glacier surface elevation change and mass balance is the C-band penetration into ice and snow (Gardelle et al., 2013; Kääb et al., 2015, 2012). Before evaluating surface elevation changes and mass balance, a correction for the C-band penetration into ice and snow was applied to all sub-basins. The exact correction of the SRTM C-band penetration depth is difficult to determine because of the lack of knowledge on the precise snow/ice conditions at the time of SRTM data acquisition (Nuth and Kääb, 2011). This study similarly estimated the penetration as in the previous studies (Gardelle et al., 2013, 2012a,b), i.e., by comparing SRTM-C with SRTM-X data over glaciers in each sub-basin separately. Fortunately, the release of 30 m SRTM-C data (previously only available in 90 m resolution outside the United States (US)) enabled us to avoid any re-sampling discrepancies in comparison with the SRTM-X data, which was already available with a 30 m resolution. However, the coverage of the penetration estimation was limited to the narrow swath of SRTM-X data. The derived C-band penetration is also an approximation, as the SRTM X-band energy also tends to penetrate into ice and snow (Gardelle et al., 2012a,b). In the central Karakoram, the estimated bias was expected to be $-0.10$ m w.e.a$^{-1}$ (Rankl and Braun, 2016). These estimates have still a limitation of data acquisition in different years because radar penetration varies with time in a year. Therefore, we used the X-band penetration calculated in the Karakoram region as the penetration bias. The C-band penetration was calculated for each sub-basin to derive surface elevation change estimates. The penetration values fluctuate throughout the Indus Basin and increase as elevation increases. On average, the penetration values in the Hindu Kush, Himalaya, and Karakoram are estimated to be 2.7 ± 1.3 m, 1.7 ± 1.1 m and 2.4 ± 1.3 m, respectively. The values of penetration increased heterogeneously from an elevation above 4500 m a.s.l. at a threshold of an approximately 2 m and reached up to 10 m in the accumulation area calculated within 100 m elevation bins. The C-band penetration bias in the glacier surface elevation change was removed using the average values within each 100 m elevation bin for all sub-basins. The bias in penetration as in the Karakoram due to the SRTM-X and C-band ($E_p$) was added to the uncertainty in the annual mass balance results (Bolch et al., 2017).

### 3.3. Glaciers surface elevation change and mass balance estimation

After the DEM co-registration, the corrected RGI6.0 glacier boundaries were used to extract the SRTM DEM and ALOS DEM for the glacierized region. The glacier areas of the SRTM DEM were subtracted from those of the ALOS DEM to obtain the glaciers surface elevation changes (Eq. (1)). These changes were used to estimate the annual glacier mass balance.

$$\Delta H = H_{ALOS} - H_{SRTM} \quad (1)$$

The SRTM DEM was acquired in February 2000 assuming it as representative of the post-ablation season of 1999 (Bolch et al., 2017). Although, some researchers have considered the effect of accumulation,

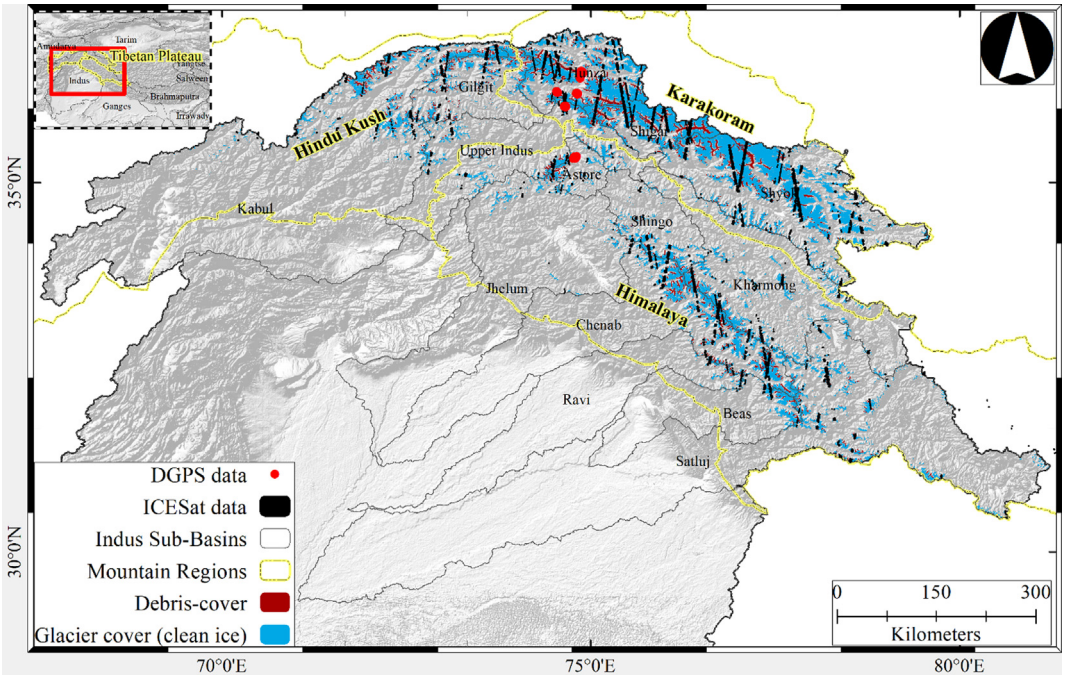


**Fig. 1.** Location map of the study area. The map shows sub-basins, mountain ranges and glacier outlines (clean ice and debris-covered) in the Indus Basin. The Map also shows dGPS and ICESat data footprints that were used for validation of glacier surface elevation changes.

in the current study it is considered as negligible and is equivalent to the SRTM X-band penetration to remove the bias in addition to the calculated C-band penetration. We base this assumption on the fact that precipitation in the 1999–2000 winter was the lowest between 1975 and 2005 (Sarfaraz et al., 2015). Similarly the snow cover in February 2000 was the lowest in this month between 2000 and 2017 (NASA Earth Observatory, 2017). The assumption that SRTM represents the ablation period of 1999 is considered to compensate for SRTM X-band penetration bias. The ALOS DEM was generated using images acquired from January 2006 to May 2011 by the PRISM sensor aboard the ALOS satellite. Unfortunately, the exact date of the data acquisition is unknown for the ALOS DEM. We assume that the ALOS data are uniformly distributed in space and time in the region. This assumption allows us to use 2008 as the median year (considering that negligible data were acquired during 2011) with the unknown dates "t" having a standard deviation of 1 year. However, this assumption introduces some uncertainty, in extreme cases, the data might have been acquired in either 2006 or 2010 (assuming negligible data obtained in 2011 because the satellite stopped acquiring data from April). The uncertainty in the annual glacier change was derived considering both of these cases, as the shift represents either six years or ten years. The six- and ten-year changes were subtracted (absolute values) from the assumed eight-year change and averaged for possible uncertainty ($E_{UO}$) (over- or under-estimation) in the estimated surface elevation change, as described in Eqs. 2–4.

$$UE = Absolute\left(\frac{H_{ALOS} - H_{SRTM}}{8} - \frac{H_{ALOS} - H_{SRTM}}{6}\right) \quad (2)$$

$$OE = Absolute\left(\frac{H_{ALOS} - H_{SRTM}}{8} - \frac{H_{ALOS} - H_{SRTM}}{10}\right) \quad (3)$$

$$E_{UO} = \frac{UE + OE}{2} = \pm Error \quad (4)$$

where UE and OE represent underestimation and overestimation, respectively. This represents a ± 2-year uncertainty in the derived results. These estimates also contain seasonal uncertainty associated with the unknown data acquisition dates, which cannot be directly estimated. We expect the seasonal and annual changes in the observed study period to be homogenous considering the insignificant changes in summer and winter temperature and precipitation (Muhammad and Tian, 2016), and we have added this uncertainty to the results, which increase the uncertainty to ± 2.5 years ($E_t$).

The density of the glacier ice varies from ablation to accumulation zone. The derived surface elevation difference was converted into water equivalent (w.e.) for glacier ice below and above 20° and 25° slope using SRTM 30 m data. The slope thresholds are assumed following Hewitt (2014, 2011) and Immerzeel et al. (2013). Practically, the exact variable density quantification is nearly impossible. For debris-covered and debris-free ice on slopes ≤25° which is mostly in the ablation area, 900 ± 60 kg m$^{-3}$ and 850 ± 60 kg m$^{-3}$ densities were applied, respectively. For debris-free ice on slopes ≤25°, we used density of 850 ± 60 kg m$^{-3}$ because some of the ice is not fully compacted and have low density (Huss, 2013). Most of the glacier surface ice on slopes steeper than approximately 25° is firn and snow (Immerzeel et al., 2013; Khan et al., 2015). The firn and snow on slopes > 25°, which eventually becomes part of a glacier, was assigned a density of 600 ± 60 kg m$^{-3}$ (Cuffey and Paterson, 2010). Although the above criteria have the possibility of some unknown uncertainty in association with the movement of ice from the accumulation zones to the ablation zones, such uncertainty is assumed negligible and unquantifiable. The density of the glacier ice below the upper layer is usually quite high, while the upper layer density is more important for glacier surface elevation change. This assumption may produce some uncertainty in the estimated mass balance. Therefore, we assume an uncertainty of ± 7% ( ± 60 kg m$^{-3}$) (Huss, 2013). The average mass balance results were estimated for each sub-basin and mountain range in the Indus Basin.

Some data are missing from both the SRTM and ALOS acquired DEMs. This restricts the coverage of both the DEMs to about 63.22% of the glacierized region. These data voids are almost entirely located in the accumulation zones due to the poor performance of stereo data on the bright surface (snow), steep slopes (~80% of the data above 25° slope are voids) and clouds, and by SRTM in steep terrain. The elevation changes are either positive or relatively very small in these areas in contrast to the significant thinning in the ablation zones. Neglecting the data voids could produce a negative bias in the average mass balance

results (Bolch et al., 2017; Pieczonka and Bolch, 2015). Therefore, thickness change was estimated in the region with data voids by averaging the values of existing pixels assuming the void pixels experienced the mean elevation change of the measurable pixels in the same altitude interval (Gardelle et al., 2012a,b). The mean error in the elevation change was derived from the available pixels with values within the most data void regions (dividing the elevation change by the total number of available pixels in the voids). This error was applied to the average mass balance as possible uncertainty.

### 3.4. Inter-comparison of ALOS, SRTM, ICESat and dGPS data and uncertainty estimation

In 2014 and 2015, six glaciers were surveyed to obtain precise ground-based dGPS measurements and to validate the surface elevation changes derived from the ALOS and SRTM comparison. The dGPS data were compared with ICESat data (2003–2008) for cross-validating the annual surface elevation change (ALOS vs. SRTM) within the areas with dGPS data, assuming homogenous temporal changes between 2000 and 2015 with respect to the insignificant changes in climate data during this period (Muhammad and Tian, 2016). The comparison of thickness change in 2003 to 2008 and 2008 to 2015 for Sachen and Burche glaciers (Muhammad and Tian, 2016) further verify the insignificant change in climate data in this period. ICESat data within a 60 m diameter were re-measured at 3–8 well-distributed locations as described by Muhammad and Tian (2016). Four glaciers were measured in the Hunza sub-basin, and one glacier each was measured in the Upper Indus sub-basin and the Astore sub-basin. The ALOS vs SRTM and ICESat vs SRTM comparison is shown in Table 1. The dGPS-based validation of the ICESat data is shown in Table 2. The dGPS data (compared to ICESat and SRTM) is confined exclusively to the ablation zones of the glaciers and should only be compared with the data sets in Table 2. Results for the Burche and Sachen glaciers have already been published (Muhammad and Tian, 2016), whereas, data on the other glaciers have not been previously published. For comparison, the thickness changes were calculated for identical geolocations using ALOS and SRTM data and were compared to those calculated using dGPS and SRTM data (Muhammad and Tian, 2016). The results in Table 2 also verify ICESat data-based validation, as shown in Table 1, and the difference in elevation change values of Sachen and Burche glaciers lie within the expected range. The dGPS-based annual elevation changes are higher due to the limited survey in the ablation zone. Consequently, the dGPS-based validation data over Barpu, Ghulkin, Minapen, and Passu contains differences of about 20 to 30 cm $a^{-1}$ from the SRTM and ALOS-based results in the annual surface elevation change. The results in Tables 1 and 2 should not be compared with the mass balance results in Table 4 and the data in these tables are limited to ICESat and dGPS, respectively. The difference of column 2 and 3 in Table 1 is equal to the difference of ALOS (assumed as acquired in 2008) and ICESat (2008–2009), which is the possible uncertainty in the assumption of the ALOS data acquisition time. Table 2 is a double check of the uncertainty as in Table 1 but not considered for any further analysis. The maximum bound of the uncertainty was estimated by equation (5) (Bolch et al., 2017; Muhammad et al., 2019).

$$E = E_{\Delta h} + E_t + E_p + E_m \quad (5)$$

where $E_{\Delta h}$, $E_t$, $E_p$, $E_m$ are uncertainty associated with thickness change, the difference in data acquisition time, penetration and density assumption, respectively.

**Table 1**
Comparison of surface elevation changes (m $a^{-1}$) derived from ALOS vs. SRTM data and ICESat vs. SRTM estimates. The coverage is limited to areas where the ICESat data overlap with SRTM and ALOS data (each ICESat footprint was compared to 3–6 pixels within a diameter of 60 m).

| Basin Name | ALOS VS SRTM (m $a^{-1}$) | ICESat VS SRTM (m $a^{-1}$) | No of Data Points |
|---|---|---|---|
| Astore | −0.44 ± 0.13 | −0.33 ± 0.15 | 29 |
| Beas | −0.15 ± 0.13 | −0.24 ± 0.20 | 41 |
| Chenab | −0.60 ± 0.05 | −0.52 ± 0.06 | 719 |
| Gilgit | −0.13 ± 0.19 | −0.25 ± 0.17 | 151 |
| Hunza | −0.21 ± 0.13 | −0.30 ± 0.15 | 577 |
| Indus Upper | −0.51 ± 0.22 | −0.56 ± 0.22 | 141 |
| Jhelum | −0.33 ± 0.17 | −0.48 ± 0.23 | 13 |
| Kabul | −0.26 ± 0.15 | −0.38 ± 0.17 | 355 |
| Kharmong | −0.32 ± 0.05 | −0.37 ± 0.05 | 511 |
| Ravi | −0.64 ± 0.26 | −0.66 ± 0.24 | 39 |
| Satluj | −0.67 ± 0.16 | −0.69 ± 0.18 | 339 |
| Shigar | 0.01 ± 0.07 | −0.01 ± 0.08 | 576 |
| Shingo | −0.42 ± 0.07 | −0.31 ± 0.08 | 90 |
| Shyok | −0.08 ± 0.04 | 0.00 ± 0.04 | 1386 |

**Table 2**
Comparison of glacier surface elevation changes (m $a^{-1}$) derived from ALOS vs. SRTM data with dGPS data and ICESat data.

| Glacier Name | Basin Name | ALOS VS SRTM (m $a^{-1}$) | dGPS VS ICESat (m $a^{-1}$) | dGPS vs SRTM (m $a^{-1}$) | No of Data Points |
|---|---|---|---|---|---|
| Sachen | Astore | −0.15 ± 0.05 | −0.26 ± 0.02 | −0.08 ± 0.04 | 68 |
| Burche | Indus (Up) | −0.24 ± 0.10 | −0.15 ± 0.03 | −0.17 ± 0.08 | 57 |
| Ghulkin | Hunza | +0.18 ± 0.13 | +0.07 ± 0.08 | +0.10 ± 0.14 | 04 |
| Passu | Hunza | −1.51 ± 0.12 | −1.66 ± 0.92 | −1.76 ± 0.08 | 04 |
| Barpu | Hunza | −0.80 ± 0.07 | −0.64 ± 0.15 | −0.51 ± 0.04 | 09 |
| Minapen | Hunza | −2.01 ± 0.28 | – | −2.20 ± 0.30 | 28 |

## 4. Results

### 4.1. Comparison results of updated glacier inventory

The difference of glacier inventory in this study compared to ICIMOD and RGI (version 4.0 and 6.0) is shown in Table 3. The reason for selecting these inventories was the full spatial coverage of the study area glaciers. The RGI version 4.0 and 6.0 (version 6.0 is similar to 5.0 for the study region) were compared to assess the improvement in the current version. The RGI4.0 and ICIMOD inventories exhibit overall underestimations when compared to the glacier outlines in this study, but the RGI6.0 inventory presents a significant improvement over its previous version. The RGI4.0 uncertainties (difference with our inventory) for the Astore and Gilgit sub-basins are significantly reduced in RGI6.0 from +53.8% and −26.3% to +2.5% and +3.7%, respectively. For the Hunza sub-basin, the 5.2% underestimation in RGI4.0 shifts to an overestimation of the same magnitude in RGI6.0. Note, positive signs represent overestimations, and negative signs represent underestimations. The remaining uncertainty of approximately 5% (at most) in the glacier outlines in the RGI6.0 glacier inventory was assumed as uncertainty constrained by Landsat satellite data quality. The overlap ratio of RGI6.0 also shows considerable precision (Table 3). The spatial differences (over/underestimations) in the glacier outlines in RGI6.0 compared to those in this study are also shown in the maps in Supplementary Figures S1-S3. Some examples of the spatial difference in glacier boundaries of this study and RGI6.0 from Astore, Gilgit, and Hunza sub-basins are shown in Fig. 2. The main difference in the boundaries is owing to the misclassification of debris-covered areas that were mapped in this study and used for the mass balance estimation. The total glacier cover area in the improved inventory of the Indus Basin were 26,029 $km^2$, including 2605 $km^2$ of debris cover (debris cover is almost 10% of the total glacier cover).

### 4.2. Mass balance estimation

The mass balance of glaciers in each sub-basin are listed in column 3

**Table 3**
Overlap ratios and common areas for the areas of glaciers in select sub-basins between the results of this study and the ICIMOD, RGI4.0, and RGI6.0 glacier inventories. Overlap ratio values of RGI6.0 in comparison to our study are highlighted.

| Comparison | Area (Sq. Km.) | | | Overlap ratio | | | Common area | | |
|---|---|---|---|---|---|---|---|---|---|
| | Astore | Gilgit | Hunza | Astore | Gilgit | Hunza | Astore | Gilgit | Hunza |
| This Study | **251.7** | **1139** | **4053** | 1 | 1 | 1 | 251.7 | 1139 | 4053 |
| ICIMOD | **239.3** | **879** | **2745** | 0.86 | 0.80 | 0.78 | 211.6 | 799 | 2617 |
| RGI4.0 | **545** | **839** | **3836** | 0.58 | 0.62 | 0.73 | 216.4 | 603 | 2893 |
| RGI6.0 | **257.9** | **1181** | **4262** | **0.89** | **0.92** | **0.93** | 227.3 | 1063 | 3850 |

and 4 of Table 4. One of the most important findings of this study is the sensitivity of mass balance to density assumptions. In mass balance method I we used a constant density of 850 ± 60 kg m$^{-3}$. In mass balance method II, a density of 850 ± 60 kg m-3 for debris-free ice with a slope ≤25°, 600 ± 60 kg m$^{-3}$ for debris-free ice with a slope > 25° and 900 ± 60 kg m$^{-3}$ for debris-covered ice. Mass balance method III considers the same ice density assumption as in method I at the slope threshold of 20°. In method IV, the glacier is divided into two classes i.e. below and above 20° slope and a density of 900 ± 60 kg m$^{-3}$ was applied to glacier ice with slopes ≤20° and 800 ± 60 kg m$^{-3}$ of density was assumed for glacier ice with slopes > 20°. The surface elevation changes (m) and annual mass balance values derived from the method I are labelled in selected sub-basins are shown in Fig. 3. In mass balance method III, the density assumption is similar as in method II but the slope cut off is 20°. Mass balance method IV makes only two density assumptions that are 900 ± 60 kg m$^{-3}$ for debris-covered and debris-free ice ≤20° slope and 800 ± 60 kg m$^{-3}$ for slopes > 20°. The average density assumption (as compared to the other three-density assumption criteria) produces a bias between −0.20 and 0.09 m w.e.a$^{-1}$. The bias is maximum in the densely glacierized sub-basins of the Karakoram. The bias in the Hindu Kush and Himalaya is comparable. Overall, the bias due to the constant density assumption results in a reduction of the imbalance by 35%.

Here we describe results obtained from mass balance method II as in Table 4. All the sub-basins of the Indus Basin show negative mass balance with variable rates. The Hunza and Shigar sub-basins (Karakoram Region) exhibited negligible mass losses. The mass balance of Shyok sub-basin in the eastern Karakoram is more negative compared to the other sub-basins in the Karakoram. In contrast, most negative mass balance (more negative than −0.34 m w.e. a$^{-1}$) is observed in the Chenab, Jhelum and Ravi sub-basins (in the south of the western Himalaya). The overall mass balance of the Hindu Kush Himalaya region of the Indus Basin is comparable. The glacier mass balance values varied in the Karakoram region from east to west and were more heterogeneous in the Hindu Kush region, but were homogenously negative in the Himalaya sub-basins.

The estimated mass change from mass balance method II was converted into Gt a$^{-1}$, as shown in column 5 of Table 4. On the regional scale, almost half of the mass losses came from the Himalaya although the glacier coverage in this region is less than one-third of the Indus Basin. On the other hand, total mass losses in the Hindu Kush is half of the Karakoram covering only about 12% of the glacierized region. About 40%, 20% and 13% of the mass losses in the Indus Basins are from the Shyok, Chenab and Kabul sub-basins, respectively. The remaining 27% are from the rest of the eleven sub-basins. As a whole, the Indus Basin contributes approximately 0.014 ± 0.016 mm a$^{-1}$ to the global mean sea-level equivalent.

## 5. Discussion

Variety of earlier research work focused on the glacier mass balance in the Indus Basin, this paper presents a new result on the glacier mass losses in the entire Indus Basin. We used variable glacier ice density for the volume to mass change estimation as the average values produce significant bias, particularly for the densely glacierized basins. Our results of comparing various density assumptions (as in Table 4) for volume to mass change estimation show significant positive bias

**Table 4**
Mass balance of the sub-basins of the Indus Basin and regions (the Karakoram, Himalaya, and the Hindu Kush). In mass balance I, an average density of 850 ± 60 kg m$^{-3}$ was assumed for the whole glacierized region. In mass balance II, we consider a density of 850 ± 60 kg m$^{-3}$ for debris-free ice (slope ≤25°), 600 ± 60 kg m$^{-3}$ for debris-free ice (slope > 25°) and 900 ± 60 kg m$^{-3}$ for debris-covered glacier regions. Mass balance III uses same density criteria as in I revising the slope threshold to 20°. Mass balance IV considers a density for ice ≤20° of 900 ± 60 kg m$^{-3}$ and > 20° of 800 ± 60 kg m$^{-3}$.

| Basin/ Region Name | Glacier area (Km$^2$) | Mass balance I (m w.e.a$^{-1}$ ± 2σ) | Mass balance II (m w.e.a$^{-1}$ ± 2σ) | Mass balance III (m w.e.a$^{-1}$ ± 2σ) | Mass balance IV (m w.e.a$^{-1}$ ± 2σ) | Min. Diff. between method I and others | Max. Diff. between method I and others | Mass loss in Gt a$^{-1}$ |
|---|---|---|---|---|---|---|---|---|
| Astore | 252 | −0.29 ± 0.22 | −0.31 ± 0.24 | −0.34 ± 0.25 | −0.30 ± 0.22 | −0.01 | −0.05 | −0.08 ± 0.06 |
| Beas | 506 | −0.15 ± 0.15 | −0.20 ± 0.19 | −0.22 ± 0.19 | −0.17 ± 0.16 | −0.02 | −0.07 | −0.10 ± 0.09 |
| Chenab | 2656 | −0.33 ± 0.26 | −0.37 ± 0.30 | −0.39 ± 0.31 | −0.34 ± 0.27 | −0.01 | −0.06 | −0.97 ± 0.78 |
| Gilgit | 1139 | −0.09 ± 0.12 | −0.14 ± 0.17 | −0.16 ± 0.18 | −0.11 ± 0.13 | −0.02 | −0.07 | −0.16 ± 0.18 |
| Hunza | 4053 | 0.11 ± 0.15 | −0.02 ± 0.12 | −0.05 ± 0.13 | 0.14 ± 0.14 | 0.03 | −0.16 | −0.09 ± 0.49 |
| Indus Upstream | 1013 | −0.01 ± 0.13 | −0.07 ± 0.15 | −0.09 ± 0.16 | −0.03 ± 0.13 | −0.02 | −0.08 | −0.19 ± 0.45 |
| Jhelum | 252 | −0.41 ± 0.32 | −0.34 ± 0.31 | −0.32 ± 0.32 | −0.35 ± 0.32 | 0.06 | 0.09 | −0.06 ± 0.06 |
| Kabul | 2090 | −0.26 ± 0.24 | −0.30 ± 0.25 | −0.32 ± 0.27 | −0.28 ± 0.24 | −0.02 | −0.06 | −0.63 ± 0.53 |
| Kharmong | 1465 | −0.17 ± 0.22 | −0.26 ± 0.24 | −0.30 ± 0.25 | −0.19 ± 0.22 | −0.02 | −0.13 | −0.37 ± 0.35 |
| Ravi | 157 | −0.43 ± 0.27 | −0.44 ± 0.27 | −0.46 ± 0.25 | −0.42 ± 0.25 | −0.01 | −0.03 | −0.07 ± 0.04 |
| Satluj | 1520 | −0.20 ± 0.23 | −0.25 ± 0.24 | −0.28 ± 0.25 | −0.22 ± 0.23 | −0.02 | −0.08 | −0.38 ± 0.36 |
| Shigar | 2985 | 0.11 ± 0.15 | −0.01 ± 0.13 | −0.09 ± 0.15 | 0.14 ± 0.14 | 0.03 | −0.2 | +0.04 ± 0.42 |
| Shingo | 628 | −0.18 ± 0.23 | −0.26 ± 0.25 | −0.29 ± 0.25 | −0.21 ± 0.24 | −0.03 | −0.11 | −0.16 ± 0.16 |
| Shyok | 7313 | −0.21 ± 0.21 | −0.26 ± 0.24 | −0.28 ± 0.24 | −0.23 ± 0.22 | −0.02 | −0.07 | −1.88 ± 1.71 |
| Himalaya | 7727 | −0.25 ± 0.22 | −0.30 ± 0.23 | −0.33 ± 0.23 | −0.26 ± 0.22 | −0.01 | −0.08 | −2.29 ± 1.75 |
| Hindu Kush | 3129 | −0.21 ± 0.23 | −0.25 ± 0.24 | −0.28 ± 0.26 | −0.22 ± 0.24 | −0.01 | −0.07 | −0.78 ± 0.77 |
| Karakoram | 15,173 | −0.03 ± 0.17 | −0.13 ± 0.18 | −0.16 ± 0.17 | −0.05 ± 0.15 | −0.02 | −0.13 | −1.72 ± 2.53 |

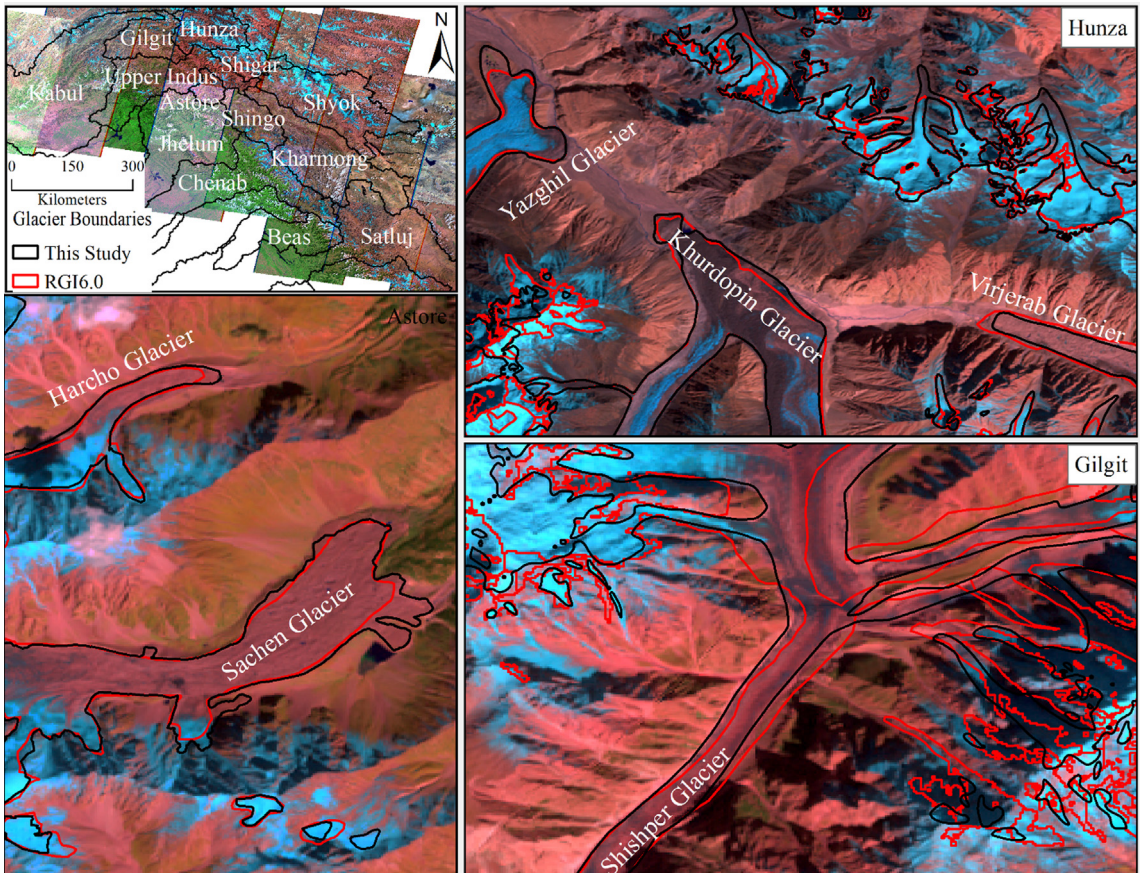


**Fig. 2.** Difference in glacier outlines at selected locations of Astore, Gilgit and Hunza sub-basins derived in this study (black lines) and RGI6.0 (red lines). (For interpretation of the references to colour in this figure legend, the reader is referred to the web version of this article.)

particularly in the densely glacierized sub-basins of the Karakoram. We apply variable density (Huss, 2013) for different slopes and differentiate between debris-covered and debris-free ice (Hewitt, 2014; Immerzeel et al., 2013). The bias caused by the assumption of the average density of 850 kg m$^{-3}$ varied between −0.20 and 0.09 m w.e.a$^{-1}$ throughout the Indus Basin. The bias comes mainly from the thickness change and glacier cover above 20° and 25° slope where 600 kg m$^{-3}$ density was assumed. The glacier cover area above slopes of 25° is approximately more than 40% of the whole glacierized region, but the bias is more concentrated in the Karakoram and adjacent region where the magnitude of thickness change of glacier ice above 25° is higher.

Data voids may also produce uncertainty in the mass balance results. Significant voids (~80%) in area with a slope >25° may produce a large uncertainty in the results in case of higher density assumption (density is most likely to be low in the area). However, in case of mass loss throughout the glacierized area, the possibility of ice density is higher as the surface melt exposes deeper ice with higher densities, this is however a probable scenario. The variable (low) density assumptions are more suitable in the areas where the accumulation happens in steep terrain (as in most of the Indus Basin and in some of the HKH region) and the mass losses are low or glaciers are even gaining mass. Therefore we argue that possible variable densities should be considered in such areas. The density assumption may be of less importance in areas where the mountains are less steep with less thickness change in the accumulation zones of the glaciers. Compared to the variable densities, the average density assumption produced approximately 35% less imbalance (Gt a$^{-1}$) as a whole.

In addition to data voids, unknown acquisition time of datasets may introduce some uncertainty. In this study, the upper bound of uncertainty due to unknown data acquisition time of ALOS data is ~30% of the annual mass balance results. However, this uncertainty does not affect the main issue (density assumption) highlighted in this paper. We compared our results for the Astore basin to the results from Brun et al. (2017) (Fig. 4), which we converted from their original 16 year period between 2000 and 2016 to the corresponding period of 2000 and 2008. The overall spatial elevation changes show good agreement, with differences from Bazhin glacier. Here our data indicate a surge, which has been confirmed by locals. As the surged ice is possibly melted away, this signal is likely not visible in the data of Brun et al. (2017), covering a longer period of time. Such surges are common in the Karakoram (Hewitt, 2014; Quincey et al., 2011; Steineret al., 2018) and have been reported since the 19th century (Longstaff, 1910). Historic and repeat photography (Nüsser and Schmidt, 2017; Zhu et al., 2019), ground-based measurements integrated with remote sensing imageries and DEMs can also be used to understand local-scale and long-term glacier dynamics (Muhammad et al., 2019). Few clearly visible surges can also be seen in Fig. 3 of this study where ice thickened markedly in some sections of the glacier tongue.

The derived results show an overall heterogeneous glacier mass balance pattern in the Indus Basin in the first decade of 21st century. The Karakoram region in the Indus Basin (except the Shyok sub-basin) shows negligible mass loss compared to the other parts. The average mass balance of the Karakoram is lower than the Gardelle et al. (2012a,b) result of +0.11 ± 0.22 m w.e.a$^{-1}$, but closest to the Kääb et al. (2015) result of −0.10 ± 0.06 m w.e.a$^{-1}$. The mass losses in the western and central Karakoram (Kääb et al., 2015) are negligible, in contrast to the eastern Karakoram where the mass balance values are comparable to those in the adjacent Himalaya sub-basins. Summer runoff in the Karakoram sub-basins, i.e., Hunza, Shigar, and Shyok, is equally strongly correlated with mass balance and summer temperature (measured at valley locations (Archer and Fowler, 2004)). In addition,

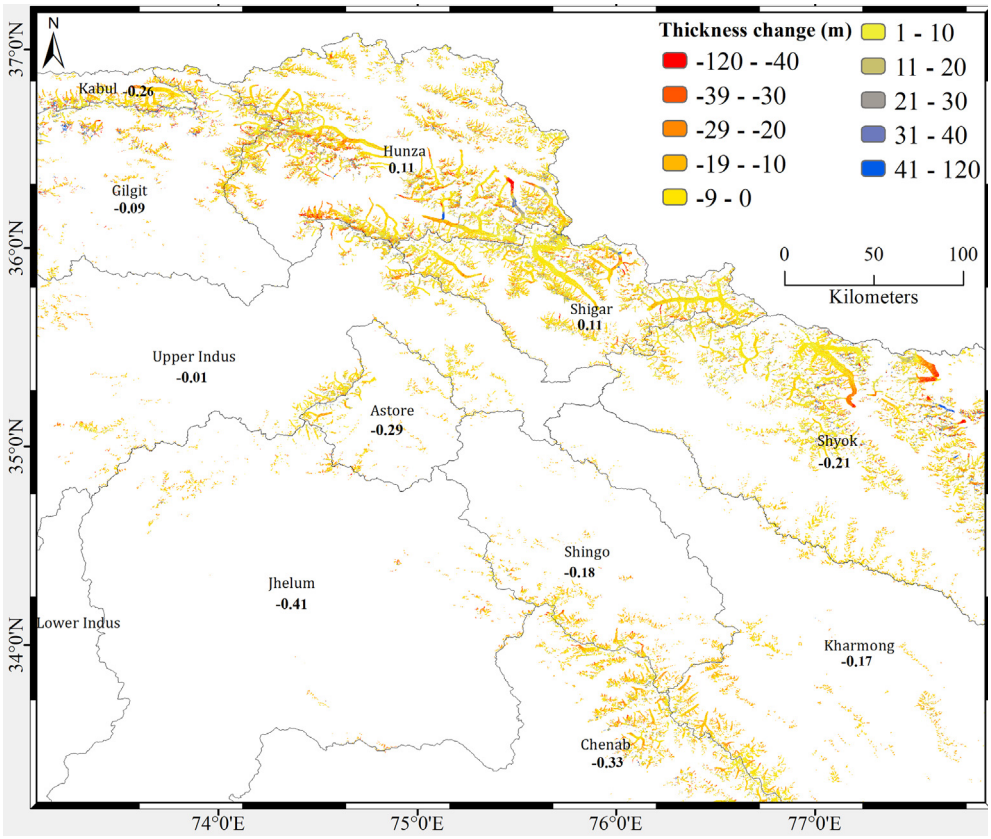


**Fig. 3.** Surface elevation change in the whole period in most of the densely glacierized regions of the sub-basins (excluding Beas, Ravi, and Satluj for better visualization) of the Indus Basin.

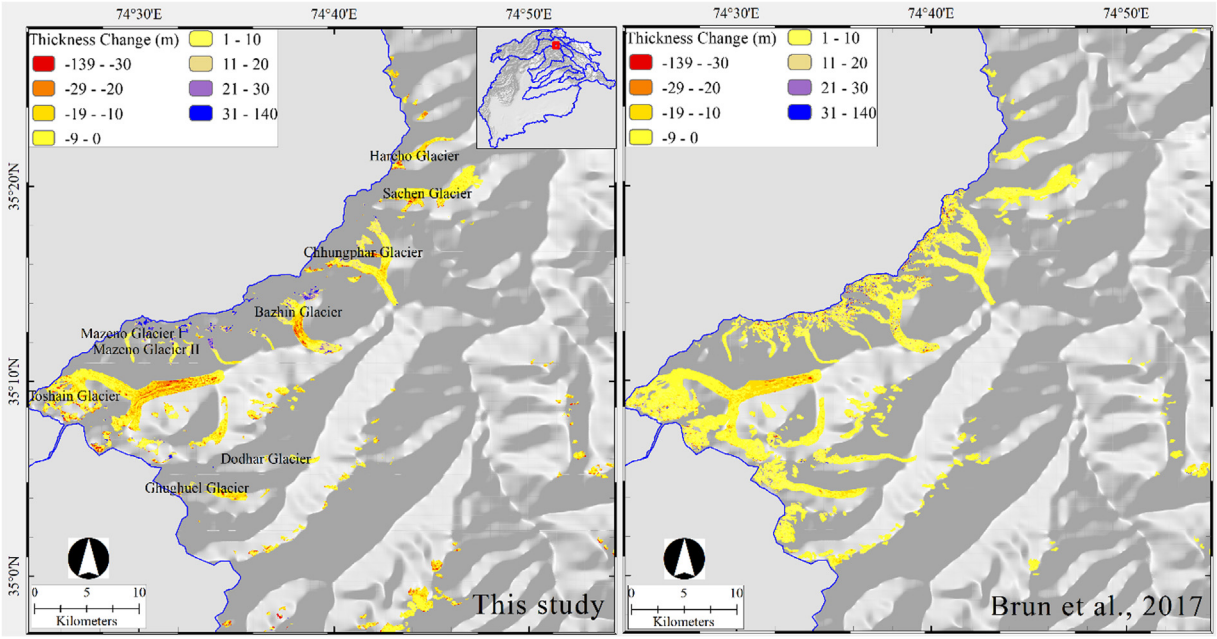


**Fig. 4.** Comparison of glaciers surface elevation change (m) between this study and Brun et al., 2017 for the glacierized area of Astore Basin (western Himalaya).

the long-term mass balance observations in the Karakoram, spanning the period 1973–2009, show negligible loss and are of the same order of magnitude as in this study (Bolch et al., 2017; Zhou et al., 2017). These studies extend the negligible and anomalously low mass loss status of the Karakoram back to the 1970s. The most recent mass balance results of the Karakoram covering the period of 2000 to 2016 show slightly less negative mass balance than estimated during 2003–2008 in the same study (Brun et al., 2017) and this paper. These results suggest that the mass loss is slower in the second decade than the first decade of this century. In addition, area changes in the central Karakoram, and the upper part of Shyok sub-basin in the Karakoram are also insignificant between 1973 and 2011 (Bhambri et al., 2013). The glaciers in the

adjacent western Kunlun Shan show a slight mass gain, observed previously for 2003–2009 (Gardner et al., 2013; Kääb et al., 2015; Neckel et al., 2014), further extended recently to the period of 2000–2014 (Lin et al., 2017).

In contrast, the retreat rates and mass losses of the Himalayan glaciers are the highest in the region. The glacier mass balance in the south of the Himalaya, including the Chenab, Jhelum, and Ravi sub-basins, is noticeably negative, comparatively to the other sub-basins. However, the losses in these sub-basins, excluding Chenab, only exert a small effect on the river flows because of the small glacial coverage. On average, glaciers in the western Himalaya was losing mass at a rate of $-0.30 \pm 0.26\,\mathrm{m\,w.e.a^{-1}}$ during the study period (Brun et al., 2017; Gardelle et al., 2013; Kääb et al., 2015). Further studies with extended spatial coverage by high-resolution satellite data and measurements of glacier ice density are recommended to reduce the possible uncertainty in glacier mass balance estimations.

The negative mass balance during the study period contributed approximately $+0.014 \pm 0.016\,\mathrm{mm\,a^{-1}}$ to global sea-level equivalent. This imbalance is equivalent to one-third of the contribution by all the glaciers in the HMA estimated during 2000–2016 by Brun et al. (2017), while covering one fourth of the total glacierized area. These results suggest that declining mass in the Indus Basin are of similar importance as in the rest of HMA. The study shows that the glacier mass losses are mostly from the Himalaya and the Hindu Kush regions in the Indus Basin. Future changes in the climate will affect glaciers and the downstream river flows, and the 21st-century projections of these changes are extremely uncertain (Immerzeel et al., 2013; Lutz et al., 2016). It is therefore crucial to collect more data in the field (Asad et al., 2017) and using remote sensing to understand the mass imbalance better.

## 6. Conclusions

This study estimated the recent glacier mass balance in the Indus Basin during the beginning of the 21st century, based on 30 m ALOS and SRTM DEM data in conjunction with separated density assumptions for debris-covered and debris-free ice above and below 20° and 25° slope and improved RGI6.0 glacier outlines. The separated density assumption reduces significant bias in volume to mass conversion constrained by thickness change of the glaciers in steep terrain (above slopes of 20° and 25°). A constant density of $850 \pm 60\,\mathrm{kg\,m^{-3}}$ in a more extended period (> 3 years as suggested by Huss (2013)) may not be useful for glaciers with significant positive thickness change. The improved and separated inventory (debris-covered and debris-free) were further classified for snow density assumption and may reduce uncertainty in total mass budget estimates. At the Indus Basin scale, the mass balance is extremely negative in the northwest of the southern sub-basins. The estimated mass balance of the glaciers in the western Himalaya are comparable to those in the Hindu Kush where the effect of density assumption is comparatively lower than the Karakoram because of the small thickness change by glacier cover above a slope of 25°. We found a contrasting pattern between east and west of the Karakoram glaciers during the study period with significant bias (between −0.20 and $0.09\,\mathrm{m\,w.e.a^{-1}}$) as compared to a constant density $850\,\mathrm{kg\,m^{-3}}$ assumption throughout the glacierized area. The density assumption must be used with caution as it depends on several factors including the magnitude of elevation changes in addition to the terrain (as considered here). The whole Indus Basin (25% glacier cover of Asia) contribution to sea-level equivalent is $+0.014 \pm 0.016\,\mathrm{mm\,a^{-1}}$ which is one-third ($0.04\,\mathrm{mm\,a^{-1}}$) of the HMA (Brun et al., 2017), in the early twenty-first century. However, continuous glaciers monitoring in the region and accurate glacier ice density assumptions for volume to mass conversion in future are critical.

## Acknowledgments

This work is funded by the National Natural Science Foundation of China (Grant no. 41530748, 41761144075, no. 41671072). We are grateful to G. Cogley and K. Hewitt or their suggestions and feedback on the earlier version of the manuscript. We highly acknowledge the freely accessible ALOS data of JAXA, ICESat GLAS data courtesy of NSIDC, Landsat data of NASA and USGS, and the SRTM elevation courtesy of NASA JPL.

## Author contributions

S.M designed the study, prepared the maps and wrote the paper. A.K. and L.T. provided suggestions and feedback on the data analysis and revised the paper. A.K. also provided glacier cover (snow and ice) data for the UIB. All the authors commented on the manuscript and edited.

## Competing financial interests

All the authors declare no competing financial interest.

## Appendix A. Supplementary data

Supplementary data to this article can be found online at https://doi.org/10.1016/j.jhydrol.2019.04.057.

## References

Archer, D., 2003. Contrasting hydrological regimes in the upper Indus Basin. J. Hydrol. 274, 198–210. https://doi.org/10.1016/S0022-1694(02)00414-6.

Archer, D.R., Fowler, H.J., 2004. Spatial and temporal variations in precipitation in the Upper Indus Basin, global teleconnections and hydrological implications. Hydrol. Earth Syst. Sci. 8, 47–61. https://doi.org/10.5194/hess-8-47-2004.

Asad, F., Zhu, H., Zhang, H., Liang, E., Muhammad, S., Farhan, S. Bin, Hussain, I., Wazir, M.A., Ahmed, M., Esper, J., 2017. Are Karakoram temperatures out of phase compared to hemispheric trends? Clim. Dyn. 48, 3381–3390. https://doi.org/10.1007/s00382-016-3273-6.

Berthier, E., Arnaud, Y., Vincent, C., Rémy, F., 2006. Biases of SRTM in high-mountain areas: implications for the monitoring of glacier volume changes. Geophys. Res. Lett. 33, L08502. https://doi.org/10.1029/2006GL025862.

Bhambri, R., Bolch, T., Kawishwar, P., Dobhal, D.P., Srivastava, D., Pratap, B., 2013. Heterogeneity in glacier response in the upper Shyok valley, northeast Karakoram. Cryosphere 7, 1385–1398. https://doi.org/10.5194/tc-7-1385-2013.

Bolch, T., Pieczonka, T., Mukherjee, K., Shea, J., 2017. Brief communication: Glaciers in the Hunza catchment (Karakoram) have been nearly in balance since the 1970s. Cryosphere 11, 531–539. https://doi.org/10.5194/tc-11-531-2017.

Brun, F., Berthier, E., Wagnon, P., Kääb, A., Treichler, D., 2017. A spatially resolved estimate of High Mountain Asia glacier mass balances from 2000 to 2016. Nat. Geosci. 10, 668–673. https://doi.org/10.1038/ngeo2999.

Cuffey, K.M., Paterson, W.S.B., 2010. The Physics of Glaciers, fourth ed. Elsevier Science & Technology Books.

Gardelle, J., Berthier, E., Arnaud, Y., 2012a. Slight mass gain of Karakoram glaciers in the early twenty-first century. Nat. Geosci 5, 322–325.

Gardelle, J., Berthier, E., Arnaud, Y., 2012b. Impact of resolution and radar penetration on glacier elevation changes computed from DEM differencing. J. Glaciol. 58, 419–422. https://doi.org/10.3189/2012JoG11J175.

Gardelle, J., Berthier, E., Arnaud, Y., Kääb, A., 2013. Region-wide glacier mass balances over the Pamir-Karakoram-Himalaya during 1999– 2011. Cryosphere 7, 1263–1286. https://doi.org/10.5194/tc-7-1263-2013.

Gardner, A.S., Moholdt, G., Cogley, J.G., Wouters, B., Arendt, A.A., Wahr, J., Berthier, E., Hock, R., Pfeffer, W.T., Kaser, G., Ligtenberg, S.R.M., Bolch, T., Sharp, M.J., Hagen, J.O., Van Den Broeke, M.R., Paul, F., 2013. A reconciled estimate of glacier contributions to sea level rise: 2003 to 2009. Science 80- (340), 852–857. https://doi.org/10.1126/science.1234532.

Haq, M., Akhtar, M., Muhammad, S., Paras, S., Rahmatullah, J., 2012. Techniques of Remote Sensing and GIS for flood monitoring and damage assessment: a case study of Sindh province, Pakistan. Egypt. J. Remote Sens. Sp. Sci. 15, 135–141. https://doi.org/10.1016/j.ejrs.2012.07.002.

Hewitt, K., 1998. Glaciers receive a surge of attention in the Karakoram Himalaya. Eos (Washington. DC) 79, 104–105. https://doi.org/10.1029/98EO00071.

Hewitt, K., 2011. Glacier change, concentration, and elevation effects in the Karakoram Himalaya, Upper Indus Basin. Mt. Res. Dev. 31, 188–200. https://doi.org/10.1659/MRD-JOURNAL-D-11-00020.1.

Hewitt, K., 2014. In: Glaciers of the Karakoram Himalaya: Glacial Environments, Processes, Hazards and Resources. Advances in Asian Human-Environmental Research. Springer Netherlands, Dordrecht. https://doi.org/10.1007/978-94-007-

6311-1.
Huss, M., 2013. Density assumptions for converting geodetic glacier volume change to mass change. Cryosphere 7, 877–887. https://doi.org/10.5194/tc-7-877-2013.
Immerzeel, W.W., Pellicciotti, F., Bierkens, M.F.P., 2013. Rising river flows throughout the twenty-first century in two Himalayan glacierized watersheds. Nat. Geosci. 6, 742–745. https://doi.org/10.1038/ngeo1896.
Kääb, A., 2005. Combination of SRTM3 and repeat ASTER data for deriving alpine glacier flow velocities in the Bhutan Himalaya. Remote Sens. Environ. 94, 463–474. https://doi.org/10.1016/J.RSE.2004.11.003.
Kääb, A., Berthier, E., Nuth, C., Gardelle, J., Arnaud, Y., 2012. Contrasting patterns of early twenty-first-century glacier mass change in the Himalayas. Nature 488, 495–498. https://doi.org/10.1038/nature11324.
Kääb, A., Treichler, D., Nuth, C., Berthier, E., 2015. Brief Communication: contending estimates of 2003–2008 glacier mass balance over the Pamir-Karakoram-Himalaya. Cryosphere 9, 557–564. https://doi.org/10.5194/tc-9-557-2015.
Khan, A., Naz, B.S., Bowling, L.C., 2015. Separating snow, clean and debris covered ice in the Upper Indus Basin, Hindukush-Karakoram-Himalayas, using Landsat images between 1998 and 2002. J. Hydrol. 521, 46–64. https://doi.org/10.1016/j.jhydrol.2014.11.048.
Kraaijenbrink, P.D.A., Bierkens, M.F.P., Lutz, A.F., Immerzeel, W.W., 2017. Impact of a global temperature rise of 1.5 degrees Celsius on Asia's glaciers. Nature 549, 257–260. https://doi.org/10.1038/nature23878.
Lin, H., Li, G., Cuo, L., Hooper, A., Ye, Q., 2017. A decreasing glacier mass balance gradient from the edge of the Upper Tarim Basin to the Karakoram during 2000–2014. Sci. Rep. 7, 1–9. https://doi.org/10.1038/s41598-017-07133-8.
Longstaff, T.G., 1910. Glacier exploration in the Eastern Karakoram. J. Geogr. 35, 622–658.
Lutz, A.F., Immerzeel, W.W., Kraaijenbrink, P.D.A., Shrestha, A.B., Bierkens, M.F.P., 2016. Climate change impacts on the upper indus hydrology: sources, shifts and extremes. PLoS One 11, 1–33. https://doi.org/10.1371/journal.pone.0165630.
Maussion, F., Scherer, D., Mölg, T., Collier, E., Curio, J., Finkelnburg, R., Maussion, F., Scherer, D., Mölg, T., Collier, E., Curio, J., Finkelnburg, R., 2014. Precipitation seasonality and variability over the tibetan plateau as resolved by the high Asia reanalysis*. J. Clim. 27, 1910–1927. https://doi.org/10.1175/JCLI-D-13-00282.1.
Memon, A.A., Muhammad, S., Rahman, S., Haq, M., 2015. Flood monitoring and damage assessment using water indices: a case study of Pakistan flood-2012. Egypt. J. Remote Sens. Sp. Sci. 18, 99–106. https://doi.org/10.1016/j.ejrs.2015.03.003.
Milner, A.M., Khamis, K., Battin, T.J., Brittain, J.E., Barrand, N.E., Füreder, L., Cauvy-Fraunié, S., Gíslason, G.M., Jacobsen, D., Hannah, D.M., Hodson, A.J., Hood, E., Lencioni, V., Ólafsson, J.S., Robinson, C.T., Tranter, M., Brown, L.E., 2017. Glacier shrinkage driving global changes in downstream systems. Proc. Natl. Acad. Sci. U.S.A. 114, 9770–9778. https://doi.org/10.1073/pnas.1619807114.
Muhammad, S., Tian, L., 2016. Changes in the ablation zones of glaciers in the western Himalaya and the Karakoram between 1972 and 2015. Remote Sens. Environ. 187, 505–512. https://doi.org/10.1016/j.rse.2016.10.034.
Muhammad, S., Tian, L., Nüsser, M., 2019. No significant mass loss in the glaciers of Astore Basin (North-Western Himalaya), between 1999 and 2016. J. Glaciol. 65. https://doi.org/10.1017/jog.2019.5.
NASA Earth Observatory Global Maps, Snow Cover. URL < https://earthobservatory.nasa.gov/GlobalMaps/view.php?d1=MOD10C1_M_SNOW/ > (accessed 1.1.17).
NATIONAL WATER POLICY 2018, 2018. Ministry of Water Resources, Government of Pakistan.
Neckel, N., Kropáček, J., Bolch, T., Hochschild, V., 2014. Glacier mass changes on the Tibetan Plateau 2003–2009 derived from ICESat laser altimetry measurements. Environ. Res. Lett. 9, 14009. https://doi.org/10.1088/1748-9326/9/1/014009.
Nüsser, M., Schmidt, S., 2017. Nanga Parbat Revisited: evolution and Dynamics of Sociohydrological Interactions in the Northwestern Himalaya. Ann. Am. Assoc. Geogr. 107, 403–415. https://doi.org/10.1080/24694452.2016.1235495.
Nuth, C., Kääb, A., 2011. Co-registration and bias corrections of satellite elevation data sets for quantifying glacier thickness change. Cryosphere 5, 271–290. https://doi.org/10.5194/tc-5-271-2011.
Pieczonka, T., Bolch, T., 2015. Region-wide glacier mass budgets and area changes for the Central Tien Shan between ~1975 and 1999 using Hexagon KH-9 imagery. Glob. Planet. Change 128, 1–13. https://doi.org/10.1016/j.gloplacha.2014.11.014.
Quincey, D.J., Braun, M., Glasser, N.F., Bishop, M.P., Hewitt, K., Luckman, A., 2011. Karakoram glacier surge dynamics. Geophys. Res. Lett. 38, L18504. https://doi.org/10.1029/2011GL049004.
RGI Consortium, 2017. Randolph Glacier Inventory–A Dataset of Global Glacier Outlines:Version 6.0: Technical Report, Global Land Ice Measurements from Space. DigitalMedia, Colorado, USA. Available from: https://www.researchgate.net/publication/329587039_Trees_record_changes_of_the_temperate_glaciers_on_the_Tibetan_Plateau_Potential_and_uncertainty [accessed Apr 23 2019], doi: https://doi.org/10.7265/N5-RGI-60.
Rankl, M., Braun, M., 2016. Glacier elevation and mass changes over the central Karakoram region estimated from TanDEM-X and SRTM/X-SAR digital elevation models. Ann. Glaciol. 57, 273–281. https://doi.org/10.3189/2016AoG71A024.
Sarfaraz, S., Masood, T., Khan, A., 2015. A Study of Anomalous Wet and Dry Years in the Winter Precipitation of Pakistan and Potential Crop Yields Vulnerability 637–644.
Shrestha, A., Agrawal, N., Alfthan, B., Bajracharya, S., Maréchal, J., van Oort, B., 2015. The Himalayan Climate and Water Atlas: Impact of climate change on water resources in five Of Asia's major River Basins. ICIMOD.
Steiner, J.F., Kraaijenbrink, P.D.A., Jiduc, S.G., Immerzeel, W.W., 2018. Brief communication: the Khurdopin glacier surge revisited-extreme flow velocities and formation of a dammed lake in 2017. Cryosphere 12, 95–101. https://doi.org/10.5194/tc-12-95-2018.
Tian, L., Yao, T., Gao, Y., Thompson, L., Mosley-Thompson, E., Muhammad, S., Zong, J., Wang, C., Jin, S., Li, Z., 2017. Two glaciers collapse in western Tibet. J. Glaciol. 63, 194–197. https://doi.org/10.1017/jog.2016.122.
Wesche, C., Riedel, S., Steinhage, D., 2009. Precise surface topography of the grounded ice ridges at the Ekströmisen, Antarctica, based on several geophysical data sets. ISPRS J. Photogramm. Remote Sens. 64, 381–386. https://doi.org/10.1016/j.isprsjprs.2009.01.005.
Winiger, M., Gumpert, M., Yamout, H., 2005. Karakorum-Hindukush-western Himalaya: assessing high-altitude water resources. Hydrol. Process. 19, 2329–2338. https://doi.org/10.1002/hyp.5887.
Zemp, M., Jansson, P., Holmlund, P., Gärtner-Roer, I., Koblet, T., Thee, P., Haeberli, W., 2010. Reanalysis of multi-temporal aerial images of Storglaciären, Sweden (1959–99) - Part 2: comparison of glaciological and volumetric mass balances. Cryosphere 4, 345–357. https://doi.org/10.5194/tc-4-345-2010.
Zhou, Y., Li, Z., Li, J., 2017. Slight glacier mass loss in the Karakoram region during the 1970s to 2000 revealed by KH-9 images and SRTM DEM. J. Glaciol. 63, 331–342. https://doi.org/10.1017/jog.2016.142.
Zhu, H., Shao, X., Zhang, H., Asad, F., Sigdel, S.R., Huang, R., Li, Y., Liu, W., Muhammad, S., Hussain, I., Grießinger, J., Liang, E., 2019. Trees record changes of the temperate glaciers on the Tibetan Plateau: Potential and uncertainty. Glob. Planet. Change 173, 15–23. https://doi.org/10.1016/j.gloplacha.2018.12.004.